Traffic collision during the breakup of an aqueous viscous compound jet

Hugo Doméjean, Jérôme Bibette, and Nicolas Bremond*
Laboratoire Colloïdes et Matériaux Divisés, CNRS, Chemistry Biology & Innovation, ESPCI Paris, PSL Research University, 10 Rue Vauquelin, F-75005 Paris, France
(Received 3 May 2016; published 20 October 2016)

Liquid jets ultimately break up into droplets through an instability driven by surface tension. For highly viscous liquids, drops are connected by cylindrical liquid filaments whose radii linearly decrease with time, thus forming drops on a string structure. For a jet composed of two aqueous phases made in air by coaxial extrusion, we observe that, for moderate Weber and capillary numbers, drops slow down with different velocities, leading to drop coalescence. The origin of the traffic collision is linked to the spatial feature of the capillary instability where capillary and viscous forces acting on the drops evolve along the jet and ultimately amplify small velocity fluctuations. The emergence of such fluctuations is related to the unstable nature of the annular coflow of liquids having contrasting viscoelastic properties. From a practical point of view, flow and actuation conditions can be adjusted to inhibit drop collision and thus drop coalescence. These findings allow then the fabrication of monodisperse submillimeter core-shell objects based on the fragmentation of compound jets made of polymer solutions that find applications for three-dimensional cell culture.

DOI: 10.1103/PhysRevFluids.1.063903

Making objects with polymers often involves extrusion of polymer melts that are known to undergo viscoelastic instabilities [1]. Polymer solutions also exhibit a rich phenomenology of drop formation during extrusion and breakup [2] that depends on rheological properties and flow features [3]. The fragmentation of polymeric jets followed by a solidification step, by immersion in a gelling bath, for example [4], allows one then to create objects that can entrap molecules or cells, which find applications in pharmaceutical or medical fields [5,6]. Making an outer layer having different physicochemical features from the core enhances the particles' versatility from encapsulation efficiency to controlled release. Besides the use of an emulsion combined with internal phase separation [7,8], solvent evaporation of a double emulsion template [9,10], and internal gelation via a *p*H modification [11,12] or by diffusion of a gelling agent from the continuous phase [13], various strategies based on an atomization step have been proposed. One implies the collision in air of drops made of aqueous and polymer solutions followed by a shell formation induced by solvent exchange [14]. However, this technique implies the use of organic solvents highly soluble in water and has not been implemented for cell encapsulation. A second way is based on the breakup of a polymer solution in air followed by an immersion of the drops in a gelling bath. The solid shell results either from the diffusion of the gelling agent towards the core of the drop containing the polymers with a precise control of the reaction time that sets the shell thickness [15] or from the deposition of polyelectrolyte layers on a gelled core that is further liquified [16,17]. Another approach relies on the fragmentation of a compound jet made by coextrusion and where the shell can be solidified in an aqueous gelling bath [18]. More specifically, the ability to form a liquid core surrounded by a solid shell in mild conditions opens new opportunities in cell culture. Indeed, cells have the capacity to grow in a multicellular structure [19], a three-dimensional configuration that is closer to *in vivo* conditions. We recently proposed a strategy for making liquid core capsules having a thin hydrogel membrane that is based on the coextrusion in air of a culture medium with cells and a polymer solution, in either dripping mode [20] or jetting mode [19]. Since viscous

*Nicolas.Bremond@espci.fr

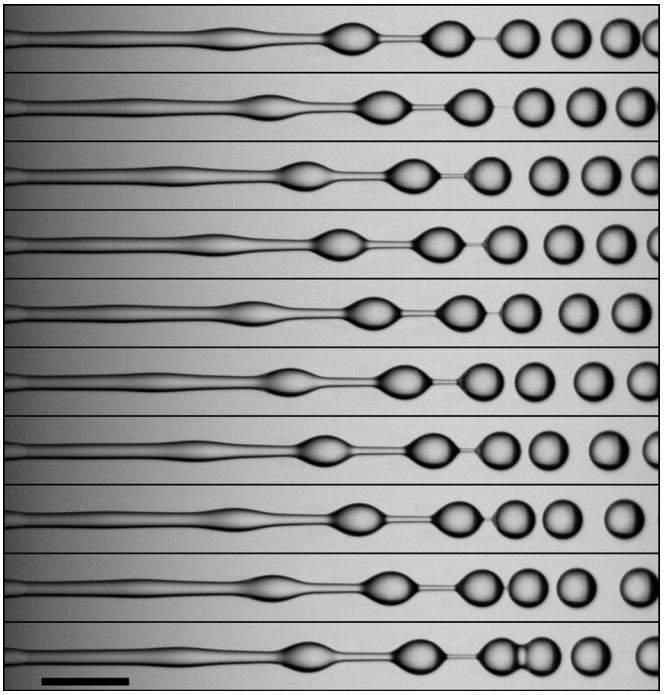

FIG. 1. Time sequence showing the fragmentation of a compound jet under harmonic perturbation where drops may eventually coalesce ($q = 125$ mL/h, $r_q = 3$, $U_p = 3$ V, and $f = 700$ Hz). The time step is 0.42 ms and the scale bar is 1 mm.

polymer solutions are used for making the hydrogel shell, viscoelastic instabilities might occur during extrusion at relatively high velocities, which are needed to form a jet, and especially because of the coflow configuration [21,22].

Most of the previous studies on stratified annular flows focused on the stability of liquid coflows in a pipe (see, e.g., [23] and references within). Experimental studies on the stability of compound jets made of miscible liquids are rather sparse [24]. Moreover, the pioneering experiments of Hertz and Hermanrud were performed at high velocities and low viscosities, thus at high Reynolds numbers, in contrast to the present conditions. On the other hand, several theoretical analyses on compound jet instability have been performed [25–27]. In this article we investigate the impact of such mixing layer instability on the breakup in air of the corresponding compound jet formed at moderate flow rates. We report the occurrence of traffic collisions of free surface waves during the fragmentation of a compound liquid jet under forced oscillations. As shown in Fig. 1, we note that even though the flow is periodically modulated, varicose wave crests travel at different velocities and drops may eventually coalesce (see video 1 in Ref. [28]). The physical origin of such a phenomenon that leads to size polydispersity of compound drops, and thus capsules, is now discussed.

The compound jet is created by using a hybrid injector made by stereolithography and glass capillary techniques. A glass capillary with an outer diameter of 1 mm and an inner one of 0.78 mm is first tapered with the help of a gravitational puller (PC-10, Narishige). Then the tip is cut by using a microforge (M900, Narishige) and finely ground. The final outer and inner diameters are 250 and 150 μm, respectively. The surface of the glass tip is made hydrophobic by silanization. The 5-mm-long glass tip is glued to a piece made in epoxy by three-dimensional printing, which allows one to generate a concentric flow of two liquids. Before exiting from the glass capillary, the outer liquid flows in a chamber equipped with a membrane that can oscillate with the help of a piezoelectric actuator (P-820, PI) by controlling frequency f and voltage U_p with a function generator (TG1000, Aim TTI).

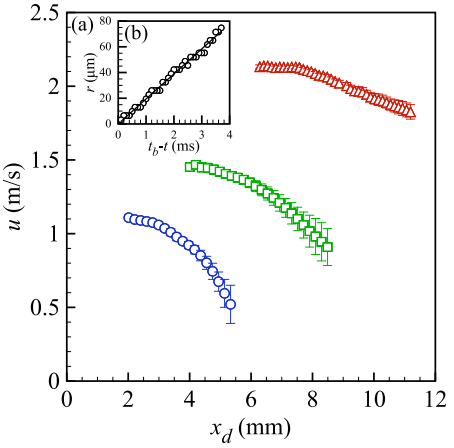

FIG. 2. (a) Evolution of the average wave and drop velocity u as a function of its location x_d along the jet axis for three total flow rate conditions: 120 mL/h (○), 140 mL/h (□), and 180 mL/h (△). (b) Time evolution of the cylindrical bridge radius r starting from the breakup time t_b along with a linear fit.

Both liquid flows are driven by syringe pumps (PhD Ultra, Harvard Apparatus). The jet is illuminated with a light-emitting diode panel (SLLUB backlight, Phlox) and observed with a high-speed camera (FastCam SA3, Photron) mounted on a macrozoom microscope (MVX10, Olympus) set horizontally. The jet fragmentation features are obtained with image processing programs developed with MATLAB.

The outer liquid is an alginate solution (sodium alginate Protanal LF200-FTS, provided by FMC Biopolymer) at 1.7 wt.% and the core one is a hydroxyethyl cellulose (HEC) solution (Sigma Aldrich) at 0.5 wt.%. The zero shear viscosity η_0 is 1.82 and 0.034 Pa s for the alginate and HEC solutions, respectively. Both polymer solutions exhibit a shear thinning behavior with a critical shear rate of 44 and 127 s^{-1} for the alginate and HEC solutions, respectively. A consequence of such a non-Newtonian behavior is the increase of the jet diameter as compared to the inner injector one. This phenomenon, known as die swelling, is linked to normal stresses built within the injector that relax within the free jet and slows down the flow [29,30]. We note that jet swelling may also result from viscous stress relaxation [31]. This jet diameter increase is accentuated for thick alginate layer. In the present experiments, the flow rate ratio between the core and the shell is set to 3 and the total flow rate ranges between 120 and 180 mL/h. As a consequence, the final jet diameter, which is reached at a distance of about two jet diameters from the end of the nozzle, varies from 170 to 200 μm. When the velocity profile has relaxed towards a uniform shape and by using mass conservation, the outer layer thickness thus varies from 11 to 13 μm. The surface tension γ between the alginate solution and air is equal to 70 mN/m. We mention that at short time scale miscible liquids with polymers exhibit a low and transient surface tension [32]. Because of the large value of surface tension between the shell solution and air, this ephemeral property is not considered later on for the analysis of the observed phenomena.

Returning to the compound jet breakup reported in Fig. 1, one can notice two important features. The first one is that the varicose wave decelerates while it propagates along the jet. This observation is supported by measurement of the wave velocity u reported in Fig. 2(a) as a function of the location x_d of the wave crest, the origin being located at the end of the nozzle. Three flow rate conditions are shown. For each condition, between 150 and 300 wave crests are followed and the average velocity and the velocity dispersion are reported. The velocity is initially constant and then decreases until the jet breakup. The deceleration is less and less pronounced as the total flow rate is increased. In addition, we note that the fluctuations of velocity are increasing while the wave propagates. Finally, the amplitude of velocity fluctuations relative to the average velocity becomes higher for low flow rates.

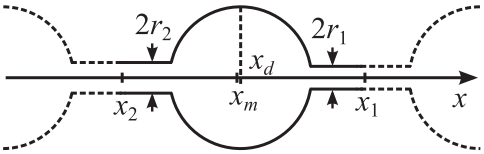

FIG. 3. Schematic of the drops on a string structure considered in the model.

The second remarkable feature is the growth of the wave amplitude via the Rayleigh-Plateau instability that leads to the formation of drops connected by cylindrical liquid filaments, a drops on a string kind of structure. As shown in Fig. 2(b), the liquid thread radius r linearly decreases with time until it ruptures. This is reminiscent of the pinch-off of a viscous liquid cylinder whose dynamics results from the competition between surface tension and viscous dissipation [33]. Indeed, the rate of thinning is given by the viscocapillary velocity γ/η that corresponds to a linear decrease of the liquid bridge radius r, i.e.,

$$r = \beta \frac{\gamma}{\eta}(t_b - t), \tag{1}$$

where t_b is the time at breakup and β is a constant that depends on the breakup regime [33]. For liquid jets composed of pure alginate solutions, knowing their surface tension and viscosity, we end up with a coefficient close to $1/6$. This value corresponds to a situation where inertia is negligible and the thread radius is homogeneous [34]. On the other hand, an exponential decrease is expected for a non-Newtonian liquid [35]. In the present experiments, the extensional rate at pinch-off is thus not high enough to trigger an elastic response and the polymer solution thus behaves as a simple viscous liquid. An effective viscosity of the compound jet can then be assessed and is equal to 0.54 Pa s for a flow rate ratio of 3.

We now propose a simple model for capturing the main features of the jet breakup. Let us consider the region of the jet where the sinusoidal varicose wave switches to drops connected to each other by liquid cylinders as sketched in Fig. 3. We choose a volume of liquid delimited by two planes normal to the jet with both located at half the length of the closest neighboring bridge of a drop, namely, x_1 and x_2. In such a way, the mass m of the corresponding volume of liquid is equal to $\rho q T = \rho \pi d_0^2 u_0 T/4$, where d_0 is the jet diameter, ρ is the volumetric mass density, q is the total flow rate, and T is the period of drop formation, which is here experimentally imposed by the oscillation frequency of the piezoelectric actuator. In the reference frame of a liquid cylinder i, the longitudinal velocity u_i induced by the filament thinning is, by mass conservation and under slenderness assumption, given by $u_i = -2(x - x_i)\dot{r}_i/r_i$, where $\dot{r}_i = dr_i/dt$. The tensile force F_i acting at one cross section i is $F_i = 2\pi r_i \gamma + \pi r_i^2 \tau_{xx}$, where the axial stress component is $\tau_{xx} = -\gamma/r_i + 3\eta \partial u_i/\partial x$ [36]. Letting x_m be the location of the center of mass of such a volume of liquid, the conservation of momentum is thus

$$m\ddot{x}_\mathrm{m} = \pi(r_1 - r_2)\gamma - 6\pi\eta(\dot{r}_1 r_1 - \dot{r}_2 r_2). \tag{2}$$

We note that the contribution of gravity into the momentum balance is neglected since its magnitude is of the order of $g x_{\max}/u_0^2$, the inverse of the Froude number, which is here around 0.05 [36]. Moreover, according to the viscous thinning dynamics of the liquid bridge (1), we finally get

$$\ddot{x}_\mathrm{m} = -\frac{4\gamma^2}{3\eta\rho d_0^2 u_0}. \tag{3}$$

Using the initial jet diameter d_0 and velocity u_0 as characteristic length and velocity scales, one ends up with the dimensionless equation

$$\ddot{x}'_\mathrm{m} = -\frac{4}{3\,\mathrm{We}\,\mathrm{Ca}}, \tag{4}$$

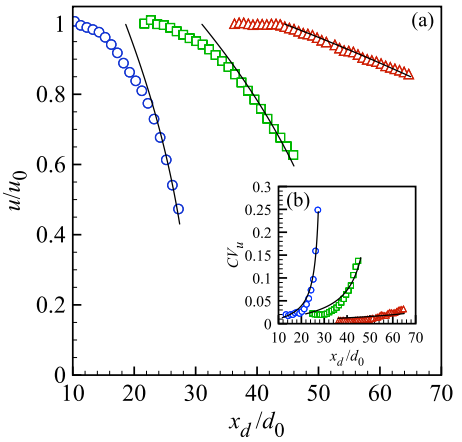

FIG. 4. (a) Comparison between the experimental evolution of the drop velocity along the jet axis (symbols) and the model prediction given by Eq. (6) (solid lines) in a nondimensional representation. Flow rate conditions are the same as in Fig. 2 and correspond to Weber numbers equal to 3.4, 5.6, and 11.2 and to capillary numbers equal to 8.5, 11.2, and 16.4, respectively. (b) Corresponding coefficients of variation of the wave velocity as a function of x_d/d_0 and defined as $CV_u = \Delta u/u$. Symbols are experimental data and the solid lines correspond to the predicted CV_u.

where $\mathrm{We} = \rho u_0^2 d_0/\gamma$ is the Weber number and $\mathrm{Ca} = u_0\eta/\gamma$ the capillary number. Considering that $\dot{x}'_{\mathrm{m}} = 1$ at $t' = 0$, the trajectory is finally

$$x'_{\mathrm{m}} = -\frac{2t'^2}{3\,\mathrm{We}\,\mathrm{Ca}} + t'. \tag{5}$$

The evolution of the velocity along the jet is thus simply

$$u' = \left(1 - \frac{8x'_{\mathrm{m}}}{3\,\mathrm{We}\,\mathrm{Ca}}\right)^{1/2} \tag{6}$$

and tends to 1, i.e., $u = u_0$, for large Weber numbers. If now there are upstream velocity fluctuations $\varepsilon = \Delta u_0/u_0$, the downstream velocity variation $\Delta u'$ can be estimated by

$$\Delta u' = u'_{+\varepsilon} - u'_{-\varepsilon}, \tag{7}$$

where the velocity extrema are

$$u'_{\pm\varepsilon} = (1 \pm \varepsilon)\left(1 - \frac{8x'}{3\,\mathrm{We}\,\mathrm{Ca}(1 \pm \varepsilon)^3}\right)^{1/2}. \tag{8}$$

The corresponding coefficient of variation CV_u of the velocity can then be evaluated, i.e., $CV_u = \Delta u'/u' = \Delta u/u$. Here we neglect the variations of d_0 due to flow fluctuations.

The experimental data shown in Fig. 2 are reported in Fig. 4(a) in a dimensionless form. The initial velocity u_0 is the one measured close to the end of the tapered glass capillary where its value is constant. The initial diameter d_0 deduced from the imposed flow rate by mass conservation matches with the measured one, meaning that the varicose wave first propagates at the fluid velocity. The corresponding Weber and capillary numbers can then be computed and range from 3.4 to 11.2 and from 8.5 to 16.4, respectively. The prediction of the model is then confronted with experimental data by assuming that the location x_m of the center of mass matches with the location x_d of the wave crest. As shown in Fig. 4(a), the model describes nicely the end evolution of the jet breakup. We stress here that there is only one adjusting parameter, namely, the location x_0 along the jet

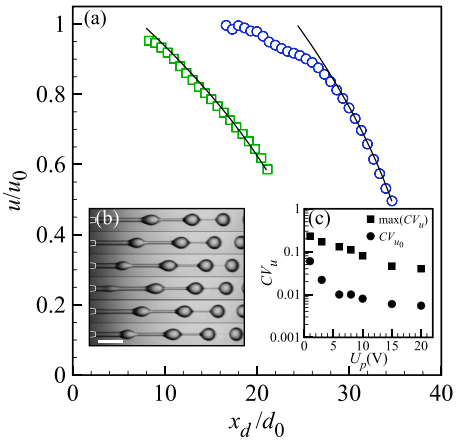

FIG. 5. (a) Comparison of the wave slowdown for two voltages U_p, imposed on the piezoelectric actuator, that sets the amplitude of the controlled velocity perturbation: 3 V (○) and 20 V (□). The flow rate is 125 mL/h and $f = 700$ Hz. The prediction of the model is also plotted. (b) Time sequence showing the fragmentation feature at a high voltage ($U_p = 20$ V); the time step is 1 ms and the scale bar is 1 mm. (c) Evolution of the initial (●) and the maximum (■) coefficient of variation of the wave velocity as a function of U_p.

where the assumption of the model is verified, i.e., when the liquid bridges become cylindrical. The amplification of velocity fluctuations is also fairly well recovered by the model [Fig. 4(b)]. The coalescence event reported in Fig. 1 is thus the result of kinematic gathering of decelerating waves due to flow velocity fluctuations that induce the contrasting slowdown, like for a traffic collision [37].

Let us now focus on the origin of initial flow fluctuations and how to minimize them. For a jet only composed of an alginate solution at a concentration of 1.15 wt.% and having a viscosity of 0.43 Pa s, i.e., close to the effective viscosity of the compound jet, and for We = 3.6, Ca = 6.4, and $U_p = 3$ V, wave crests are also decelerating but we do not observe any coalescence event during jet breakup (see video 2 in Ref. [28]). Indeed, we note that the amplitude of initial velocity variation is two times lower that the smallest We and Ca case reported in Fig. 4. Flow rate fluctuations, inherent to syringe pump driven flow, leading to a higher level of wave velocity fluctuations are the signature of a shear layer instability that develops inside the injector capillary due to the stratification of two fluids having different viscoelastic properties [21]. The increase of the liquid core viscosity with a polymer, here HEC, helps to stabilize the coflow. In addition, the use of a tapered capillary is intended to limit the length where the shear rate is elevated. A way to overcome such a behavior at moderate flow rates is to increase the amplitude of the imposed velocity modulations. An example of the drop trajectory and a time sequence of the jet breakup when the voltage U_p is set to 20 V are reported in Fig. 5. The variation of the initial coefficient of variation of the wave velocity and the maximal one reached before drop detachment as a function of U_p is also shown. We observe that CV_{u_0} quickly decreases to 1% and then slowly decreases for U_p larger than 5 V. Flow fluctuations can thus be overcome with the help of the piezoelectric actuator. The corresponding maximum CV_u behaves a bit differently since it seems to decrease exponentially until 15 V and then saturates. For high voltage, the waves and the cylindrical threads are rapidly visible close to the injector's end [Fig. 5(b)]. As shown in Fig. 5(c), the wave velocity also diminishes but with a lower deceleration than the 3-V case that corresponds to We = 4 and Ca = 9.3. The model correctly describes the wave velocity evolution once the liquid velocity is multiplied by 1.15. Therefore, the oscillation of the piezoelectric actuator not only imposes a wave mode free of background noise but also enhances the inertia of the jet. As a consequence, the probability P_c that drops coalesce during the fragmentation step decreases with U_p [Fig. 6(a)]. For that flow condition, similar to the one in Fig. 5, the drops

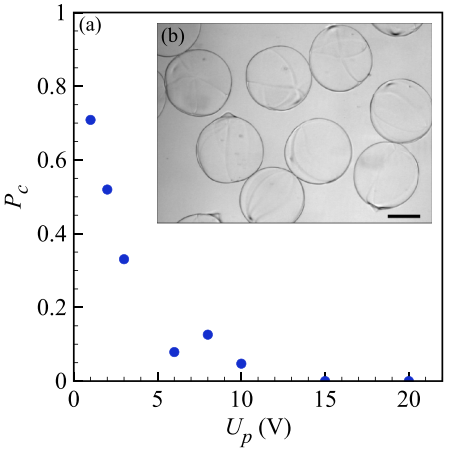

FIG. 6. (a) Probability P_c that drops coalesce during jet fragmentation as a function of piezoelectric actuator voltage U_p. The experimental conditions are similar to those in Fig. 5. (b) Photo of monodisperse aqueous core hydrogel capsules obtained after immersion of the compound drops into a calcium solution. The scale bar is 200 μm.

do not merge anymore for U_p larger than or equal to 15 V and further lead to the formation of monodisperse liquid core hydrogel capsules. An example of calibrated capsules having a size of 400 μm is reported in Fig. 6(b). These capsules are obtained by collecting the compound drops in a water bath that contains calcium ions. These divalent cations induce a sol-gel transition of the alginate solution and thus a solidification of the outer layer [38]. We note that a few surfactants in the alginate solution as well as in the gelling bath are required to obtain a proper engulfment of the compound drops and thus an efficient formation of the capsule shell [20]. A detailed characterization of the formation of submillimeter hydrogel capsules can be found elsewhere [39].

We have shown that making submillimeter liquid core capsules via an atomization step of viscous and miscible liquids may lead to capsule size polydispersity due to drop merging. The mechanism of drop coalescence is driven by the surface tension that tends to amplify velocity fluctuations that finally end up in a traffic collision phenomenon. The flow disturbances are initially amplified in the injector via a mixing layer instability between the two miscible liquids having contrasting viscoelastic properties. A way to overcome the traffic collision phenomenon is thus to increase the inertia of the liquid jet. However, this strategy might be limited by the hydraulic resistance encountered during the extrusion of such viscous solutions. The other way is then to increase the amplitude of the controlled perturbations, but this also has its own mechanical limits. Finally, even though drops do not merge during jet fragmentation, they may coalesce in flight due to kinematic gathering. This can be easily circumvented by electrically charging the drops [40] that finally repel each other before entering the gelling bath [41].

This understanding allows us to design a robust process for making calibrated compartments for three-dimensional cell culture [39]. Here we have used a weakly elastic polymer solution that finally exhibits purely viscous features when a free interface is created. An interesting extension to this work would be to incorporate elasticity into the system, which has been shown to increase the complexity of jet fragmentation [2,42]. Finally, we stress that most of the theoretical analyses of compound jet instability are carried out on a temporal basis [25–27]. However, experiments on jet breakup involving fluid flows are by construction linked to a spatially developing instability. This is the reason why we observe, at moderate Weber numbers, drop deceleration that may promote collision if velocity fluctuations exist. We thus also aim at exploring in detail the effect of a second surface tension, due to the presence of an immiscible core, on the dynamics of compound jet fragmentation, which should lead to interesting phenomena.

We thank the SIMM group, and especially Guylaine Ducouret, for having given us access to their rheometer. This work was supported by Grant No. ANR-10-BLAN-1514 from Agence Nationale de la Recherche, France.

[1] R. G. Larson, Instabilities in viscoelastic flows, Rheol. Acta **31**, 213 (1992).
[2] P. P. Bhat, S. Appathurai, M. T. Harris, M. Pasquali, G. H. McKinley, and O. A. Basaran, Formation of beads-on-a-string structures during break-up of viscoelastic filaments, Nat. Phys. **6**, 625 (2010).
[3] C. Clasen, P. M. Phillips, L. Palangetic, and J. Vermant, Dispensing of rheologically complex fluids: The map of misery, AIChE J. **58**, 3242 (2012).
[4] D. Serp, E. Cantana, C. Heinzen, U. von Stockar, and I. W. Marison, Characterization of an encapsulation device for the production of monodisperse alginate beads for cell immobilization, Biotechnol. Bioeng. **70**, 41 (2000).
[5] A. Murua, A. Portero, G. Orive, R. M. Hernandez, M. de Castro, and J. L. Pedraz, Cell microencapsulation technology: Towards clinical application, J. Control. Release **132**, 76 (2008).
[6] C. E. Mora-Huertas, H. Fessi, and A. Elaissari, Polymer-based nanocapsules for drug delivery, Int. J. Pharm. **385**, 113 (2010).
[7] A. Loxley and B. Vincent, Preparation of poly(methylmethacrylate) microcapsules with liquid cores, J. Colloid Interface Sci. **208**, 49 (1998).
[8] R. Atkin, P. Davies, J. Hardy, and B. Vincent, Preparation of aqueous core/polymer shell microcapsules by internal phase separation, Macromolecules **37**, 7979 (2004).
[9] A. S. Utada, E. Lorenceau, D. R. Link, P. D. Kaplan, H. A. Stone, and D. A. Weitz, Monodisperse double emulsions generated from a microcapillary device, Science **308**, 537 (2005).
[10] C. Berkland, E. Pollauf, N. Varde, D. Pack, and K. K. Kim, Monodisperse liquid-filled biodegradable microcapsules, Pharm. Res. **24**, 1007 (2007).
[11] Y. Morimoto, W. H. Tan, Y. Tsuda, and S. Takeuchi, Monodisperse semi-permeable microcapsules for continuous observation of cells, Lab Chip **9**, 2217 (2009).
[12] Q. S. Chen, S. Utech, D. Chen, R. Prodanovic, J. M. Lin, and D. A. Weitz, Controlled assembly of heterotypic cells in a core-shell scaffold: organ in a droplet, Lab Chip **16**, 1346 (2016).
[13] C. Kim, S. Chung, Y. E. Kim, K. S. Lee, S. H. Lee, K. W. Oh, and J. Y. Kang, Generation of core-shell microcapsules with three-dimensional focusing device for efficient formation of cell spheroid, Lab Chip **11**, 246 (2011).
[14] Y. Yeo, O. A. Basaran, and K. Park, A new process for making reservoir-type microcapsules using ink-jet technology and interfacial phase separation, J. Control. Release **93**, 161 (2003).
[15] T. Wang, I. Lacik, M. Brissova, A. V. Anilkumar, A. Prokop, D. Hunkeler, R. Green, K. Shahrokhi, and A. C. Powers, An encapsulation system for the immunoisolation of pancreatic islets, Nat. Biotechnol. **15**, 358 (1997).
[16] F. Lim and A. Sun, Microencapsulated islets as bioartificial endocrine pancreas, Science **210**, 908 (1980).
[17] V. Breguet, R. Gugerli, M. Pernetti, U. von Stockar, and I. W. Marison, Formation of microcapsules from polyelectrolyte and covalent interactions, Langmuir **21**, 9764 (2005).
[18] M. V. Sefton, R. M. Dawson, R. L. Broughton, J. Blysniuk, and M. E. Sugamori, Microencapsulation of mammalian cells in a water-insoluble polyacrylate by coextrustion and interfacial precipitation, Biotechnol. Bioeng. **29**, 1135 (1987).
[19] K. Alessandri, B. R. Sarangi, V. V. Gurchenkov, B. Sinha, T. R. Kiessling, L. Fetler, F. Rico, S. Scheuring, C. Lamaze, A. Simon *et al.*, Cellular capsules as a tool for multicellular spheroid production and for investigating the mechanics of tumor progression in vitro, Proc. Natl. Acad. Sci. USA **110**, 14843 (2013).
[20] N. Bremond, E. Santanach-Carreras, L. Y. Chu, and J. Bibette, Formation of liquid-core capsules having a thin hydrogel membrane: Liquid pearls, Soft Matter **6**, 2484 (2010).
[21] E. J. Hinch, O. J. Harris, and J. M. Rallison, The instability mechanism for 2 elastic liquids being coextruded, J. Non-Newtonian Fluid Mech. **43**, 311 (1992).

[22] R. Govindarajan and K. C. Sahu, Instabilities in viscosity-stratified flow, Annu. Rev. Fluid Mech. **46**, 331 (2014).
[23] O. Bonhomme, A. Morozov, J. Leng, and A. Colin, Elastic instability in stratified core annular flow, Phys. Rev. E **83**, 065301 (2011).
[24] C. H. Hertz and B. Hermanrud, A liquid compound jet, J. Fluid Mech. **131**, 271 (1983).
[25] A. Chauhan, C. Maldarelli, D. T. Papageorgiou, and D. S. Rumschitzki, Temporal instability of compound threads and jets, J. Fluid Mech. **420**, 1 (2000).
[26] R. V. Craster, O. K. Matar, and D. T. Papageorgiou, On compound liquid threads with large viscosity contrasts, J. Fluid Mech. **533**, 95 (2005).
[27] R. Suryo, P. Doshi, and O. A. Basaran, Nonlinear dynamics and breakup of compound jets, Phys. Fluids **18**, 082107 (2006).
[28] See Supplemental Material at http://link.aps.org/supplemental/10.1103/PhysRevFluids.1.063903 for movies.
[29] R. I. Tanner, A theory of die-swell, J. Polym. Sci. A **8**, 2067 (1970).
[30] C. Allain, M. Cloitre, and P. Perrot, Experimental investigation and scaling law analysis of die swell in semi-dilute polymer solutions, J. Non-Newtonian Fluid Mech. **73**, 51 (1997).
[31] S. L. Goren and S. Wronski, The shape of low-speed capillary jets of newtonian liquids, J. Fluid Mech. **25**, 185 (1966).
[32] D. Truzzolillo and L. Cipelletti, Off-equilibrium surface tension in miscible fluids, Soft Matter (2016), doi:10.1039/C6SM01026A.
[33] J. Eggers and E. Villermaux, Physics of liquid jets, Rep. Prog. Phys. **71**, 036601 (2008).
[34] G. H. McKinley and A. Tripathi, How to extract the newtonian viscosity from capillary breakup measurements in a filament rheometer, J. Rheol. **44**, 653 (2000).
[35] G. H. McKinley and T. Sridhar, Filament-stretching rheometry of complex fluids, Annu. Rev. Fluid Mech. **34**, 375 (2002).
[36] C. Clasen, J. Bico, V. M. Entov, and G. H. McKinley, 'Gobbling drops': The jetting-dripping transition in flows of polymer solutions, J. Fluid Mech. **636**, 5 (2009).
[37] G. B. Whitham, *Linear and Nonlinear Waves* (Wiley, New York, 1974).
[38] K. Y. Lee and D. J. Mooney, Alginate: Properties and biomedical applications, Prog. Polym. Sci. **37**, 106 (2012).
[39] H. Doméjean, M. de la Motte Saint Pierre, A. Funfak, N. Atrux-Tallau, K. Alessandri, P. Nassoy, J. Bibette, and N. Bremond (unpublished).
[40] J. M. Schneider, N. R. Lindblad, J. C. D. Hendricks, and J. M. Crowley, Stability of an electrified liquid jet, J. Appl. Phys. **38**, 2599 (1967).
[41] H. Brandenberger, D. Nüssli, V. Piëch, and F. Widmer, Monodisperse particle production: A method to prevent drop coalescence using electrostatic forces, J. Electrostat. **45**, 227 (1999).
[42] J. Li and M. A. Fontelos, Drop dynamics on the beads-on-string structure for viscoelastic jets: A numerical study, Phys. Fluids **15**, 922 (2003).